


A Universal Triangulation for Flat Tori

Francis Lazarus  

G-SCOP, CNRS, UGA, Grenoble, France

Florent Tellerie 

G-SCOP, UGA, Grenoble, France

Abstract

A result due to Burago and Zalgaller states that every orientable polyhedral surface, one that is obtained by gluing Euclidean polygons, has an isometric piecewise linear (PL) embedding into Euclidean space \mathbb{E}^3 . A flat torus, resulting from the identification of the opposite sides of a Euclidean parallelogram, is a simple example of polyhedral surface. In a first part, we adapt the proof of Burago and Zalgaller, which is partially constructive, to produce PL isometric embeddings of flat tori. In practice, the resulting embeddings have a huge number of vertices, moreover distinct for every flat torus. In a second part, based on another construction of Zalgaller and on recent works by Arnoux et al., we exhibit a *universal triangulation* with 5974 triangles which can be embedded linearly on each triangle in order to realize the metric of any flat torus.

2012 ACM Subject Classification Mathematics of computing \rightarrow Geometric topology; Mathematics of computing \rightarrow Discrete mathematics; Theory of computation \rightarrow Computational geometry

Keywords and phrases Triangulation, flat torus, isometric embedding

Digital Object Identifier 10.4230/LIPIcs.SoCG.2022.53

Related Version *Full Version:* <https://arxiv.org/abs/2203.05496>

Funding *Francis Lazarus:* This author is partially supported by the French ANR projects GATO (ANR-16-CE40-0009-01) and MINMAX (ANR-19-CE40-0014) and the LabEx PERSYVAL-Lab (ANR-11-LABX-0025-01) funded by the French program Investissement d’avenir.

Acknowledgements We warmly thank Alba Málaga, Pierre Arnoux and Samuel Lelièvre for sharing with us their constructions of flat tori and showing us how to cover their moduli space with these constructions. We are also grateful to the anonymous reviewers for their careful reading and suggestions.

1 Introduction

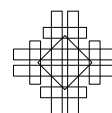
A celebrated theorem of Nash [6] completed by Kuiper [5] implies that every smooth Riemannian orientable surface has a C^1 isometric embedding in the Euclidean 3-space \mathbb{E}^3 . As a consequence one can represent and visualize faithfully in \mathbb{E}^3 the geometry of any abstract orientable Riemannian surface. An analogous result, due to Burago and Zalgaller [3], states that every orientable polyhedral surface, obtained by abstractly gluing Euclidean polygons, has an isometric piecewise linear (PL) embedding in \mathbb{E}^3 . In particular, this provides PL isometric embeddings for every flat torus, the result of the identification of the opposite sides of a Euclidean parallelogram. However, the proof of Burago and Zalgaller is partially constructive, relying on the subdivision of the polyhedral surface into an acute triangulation and on the Nash-Kuiper theorem itself, which is a priori far from constructive. The singular vertices of the polyhedral surface (where the angles at the incident polygons do not sum up to 2π) moreover deserve special treatments with several constants that are rather hard to estimate. In the case of flat tori, all these difficulties can be circumvented. In particular, a flat torus has no singular vertex. Using a simple construction of acute triangulations together with the conformal embeddings of Hopf-Pinkall [7, 2], we were able to compute PL isometric embeddings of various flat tori, including the square and the hexagonal tori.



© Francis Lazarus and Florent Tellerie;
licensed under Creative Commons License CC-BY 4.0
38th International Symposium on Computational Geometry (SoCG 2022).
Editors: Xavier Goaoc and Michael Kerber; Article No. 53; pp. 53:1–53:18
Leibniz International Proceedings in Informatics



LIPICs Schloss Dagstuhl – Leibniz-Zentrum für Informatik, Dagstuhl Publishing, Germany



In practice, the construction of Burago and Zalgaller, even including our simplifications for flat tori, produces PL embeddings with a huge number of vertices: more than 170,000 for the square torus and more than 7 millions for the hexagonal torus. Most importantly, the underlying triangulations of the resulting PL embeddings depends on the geometry (or *modulus*) of the flat tori and are pairwise non-isomorphic. Apart from the construction of Burago and Zalgaller, describing explicit PL embeddings of specific flat tori does not seem a simple task. As an illustrating example, it was only very recently that an explicit PL embedding of the square flat torus appeared in the literature [8].

We say that a triangulation of the topological torus is *universal* if, for any flat torus, it admits a geometric realization in \mathbb{E}^3 that is isometric to this flat torus. It is not clear that such a universal triangulation should exist as the moduli space of flat tori is not compact. In particular, there is no reason why any of the triangulations obtained from the method of Burago and Zalgaller would be universal. Our main result is the rather surprising existence of a universal triangulation with the description of such a triangulation of reasonable size.

► **Theorem 1.** *There exists an abstract triangulation \mathcal{T} of the torus with 5974 triangles that admits for each flat torus (in the moduli space) an embedding in \mathbb{E}^3 which is linear on each triangle of \mathcal{T} , and which is isometric to this flat torus.*

2 Background and definitions

Polyhedral surfaces

A **polyhedral surface** is a compact topological surface obtained from a finite collection of polygonal regions in the Euclidean plane by gluing their sides according to a partial oriented pairing. This pairing should be such that each side is paired at most once and two sides in a pair should have the same length. The pair orientation specifies one of the two isometries between its sides. Since every polygon can be triangulated, one can replace the polygons by triangles in this definition. The collection of triangles together with their gluing determine a **triangulation** of the surface. This triangulation is **simplicial** when there is no loop edge or parallel edges. By an **abstract triangulation** of a polyhedral surface, we mean a simplicial complex that is isomorphic to some triangulation of the polyhedral surface.

Polyhedral metric

The gluing of Euclidean polygons induces a **length metric** on the resulting polyhedral surface: the distance between any two points is the infimum of the lengths of the paths connecting the two points. There is an intrinsic definition of polyhedral surfaces that does not assume any specific decomposition into polygons. A **polyhedral metric** on a topological surface is a metric such that every point has a neighborhood isometric to a neighborhood of the apex of a Euclidean cone. In turn, a (2-dimensional) Euclidean cone is defined by coning from the origin a rectifiable simple curve on the unit sphere in \mathbb{E}^3 . The length of this curve is the total angle of the cone. A point whose conic neighborhood has total angle different from 2π is called a **singular vertex**.

Piecewise linear maps and isometries

Let S be a polyhedral surface. A map $f : S \rightarrow \mathbb{E}^3$ is said **piecewise linear** (PL) if S admits a triangulation such that the restriction of f to any triangle is *linear*, *i.e.*, it preserves barycentric coordinates. Once a triangulation of S is given, the image of its vertices in \mathbb{E}^3 determines a unique **linear map** on this triangulation by extending linearly to the images of triangles.

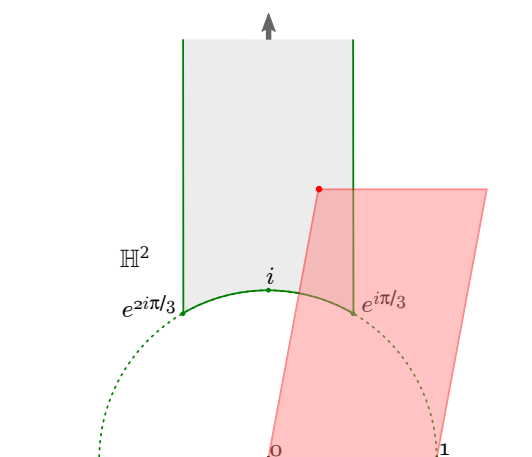
f is **piecewise distance preserving** if S admits a triangulation such that the restriction of f to any triangle is distance preserving, *i.e.*, $|f(x) - f(y)| = d_S(x, y)$ for any x, y in a same triangle. Here, $|\cdot|$ is the Euclidean norm and d_S is the polyhedral metric on S . In particular, the piecewise distance preserving map f must be **length preserving**: if $\gamma : [a, b] \rightarrow S$ is a rectifiable path, then γ and its image $f \circ \gamma$ have the same length. The map f is an **embedding** if it induces a homeomorphism onto its image $f(S)$ endowed with the restriction of the topology of \mathbb{E}^3 . In that case, $f(S)$ is naturally equipped with a length metric induced by the Euclidean metric of \mathbb{E}^3 so that the length of a path in $f(S)$ is its Euclidean length as a path in \mathbb{E}^3 .

A length preserving embedding is the same as an **isometry** between S and $f(S)$, where each surface is endowed with its own length metric, respectively polyhedral and induced by the Euclidean metric. Thus, a piecewise distance preserving embedding is the same as a **PL isometric embedding**. A map $f : S \rightarrow \mathbb{E}^3$ is said **contracting**, or **short**, if there is a constant $C < 1$ such that $|f(x) - f(y)| \leq C d_S(x, y)$ for all $x, y \in S$.

Flat tori

A **flat torus** is a polyhedral surface obtained from a Euclidean parallelogram by pairing its opposite sides. We usually consider flat tori up to re-scaling. This amounts to consider that similar parallelograms lead to the same flat torus. If (e_1, e_2) is the canonical basis of the Euclidean plane, we can thus assume that the two sides of the parallelogram are respectively e_1 and τ for some vector $\tau = \tau_1 e_1 + \tau_2 e_2$, with $\tau_i > 0$. Identifying the real plane with the complex line, we conclude that a flat torus is determined by its **modulus** $\tau = \tau_1 + i\tau_2$.

Rather than gluing the sides of a parallelogram, one can equivalently obtained the same flat torus by quotienting the Euclidean plane \mathbb{E}^2 by the rank 2 lattice $\mathbb{Z}\tau + \mathbb{Z}e_1$ acting by translations. The same lattice is generated by the vectors $(a\tau + b, c\tau + d)$, where $\begin{pmatrix} a & b \\ c & d \end{pmatrix} \in \text{SL}_2(\mathbb{Z})$ is an integer matrix with determinant 1. This lattice corresponds to the modulus $(a\tau + b)/(c\tau + d)$, where τ is again viewed as a complex number. In fact, the set of flat tori is in one-to-one correspondence with the quotient $\mathbb{H}^2/\text{SL}_2(\mathbb{Z})$, where \mathbb{H}^2 denotes the upper half-plane (the set of moduli) and $\text{SL}_2(\mathbb{Z})$ acts as above. Every flat torus has a modulus in the fundamental domain of this quotient as shown in Figure 1.



■ **Figure 1** A point (in red) in a fundamental domain of the moduli space of tori (in light grey) with the corresponding parallelogram.

3 The construction of Burago and Zalgaller

We first recall the result of Burago and Zalgaller for embedded surfaces.

► **Theorem 2** (Burago and Zalgaller [3]). *Every short C^2 embedding in \mathbb{E}^3 of a polyhedral surface can be approximated by a PL isometric embedding.*

Here, the approximation by a PL isometric map means that for any $\varepsilon > 0$ there is such a map moving the points of the short C^2 -embedding by a distance less than ε . This implies that every orientable polyhedral surface has an isometric PL embedding in 3-space. Before we give a sketch of the proof, we describe the basic construction of Burago and Zalgaller, which is a specialization of Theorem 2 to the case of a single triangle.

3.1 Embedding a triangle

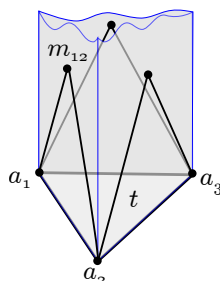
If t is a triangle in \mathbb{E}^3 and \vec{n} is a vector normal to t , then the **prism above** t is the set $\{p + \lambda\vec{n} \mid p \in t, \lambda \geq 0\}$ and the three infinite faces of this prism are its **walls**.

► **Lemma 3** ([3]). *Let $T = A_1A_2A_3$ and $t = a_1a_2a_3$ be (Euclidean) triangles in \mathbb{E}^3 such that*

- (i) *T and t are acute,*
- (ii) *$|a_ia_j| < |A_iA_j|$ for $i, j = 1, 2, 3; i \neq j$,*
- (iii) *the distance of the circumcenter ω of t to each side a_ia_j is smaller than the distance of the circumcenter Ω of T to the corresponding side A_iA_j .*

Denote by m_{ij} the point in the wall above a_ia_j at equal distance from a_i and a_j . Then, T has a PL isometric embedding in the prism above t (with respect to a normal directions) with the boundary condition that each side A_iA_j is sent to the broken line $a_ism_{ij}a_j$.

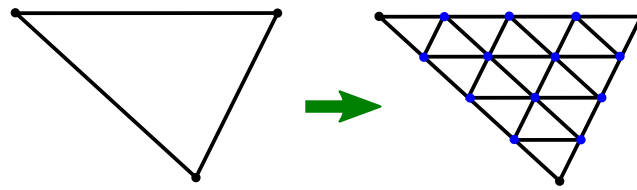
This Lemma (see Figure 2) easily implies that T has a PL isometric embedding arbitrarily



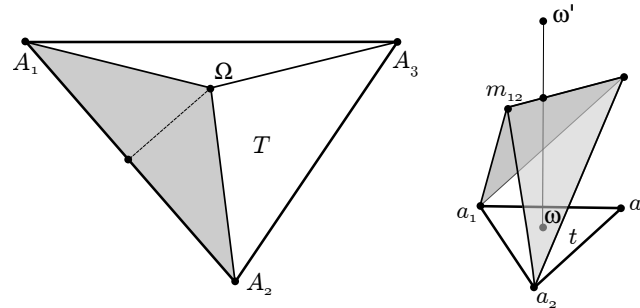
■ **Figure 2** The prism above t .

close to t . Indeed, by subdividing T and t uniformly as in Figure 3 we get similar triangles of smaller size to which we can individually apply Lemma 3. Thanks to the boundary condition in the lemma, the individual constructions fit together to form an isometric embedding of T . The constructions for the smaller triangles being homothetic to the construction for the original triangles, we get closer and closer to t as we refine the uniform subdivisions.

The triangles T and t being acute, they contain their circumcenters Ω and ω in their interior. Let \vec{n} be a unit vector normal to t and let ω' be the point vertically above ω such that $|a_1\omega'| = |A_1\Omega|$. Refer to Figure 4. Note that ω' is well-defined since by the assumptions (ii) and (iii) the circumradius $|A_1\Omega|$ of T is larger than the circumradius $|a_1\omega|$ of t . For completeness, we recall the proof of Lemma 3. Triangle T is first subdivided into three subtriangles $\Omega A_i A_j$. The goal is to fold each $\Omega A_i A_j$ above $\omega a_i a_j$ with the boundary condition

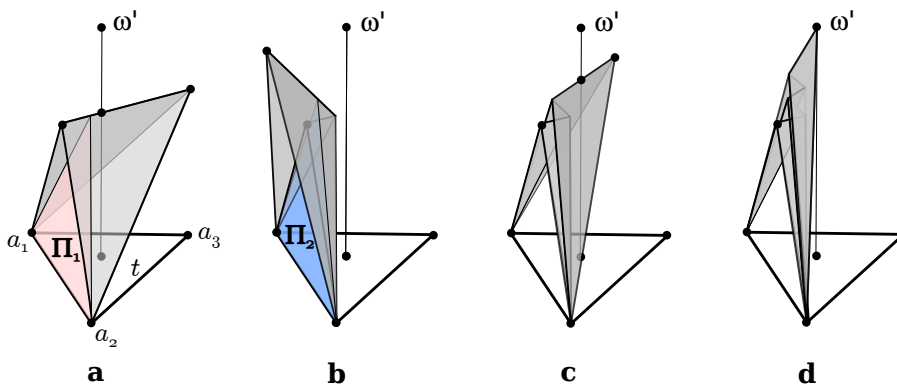


■ **Figure 3** Uniform subdivision of a triangle. The vertices of the subdivision have barycentric coordinates $(i/n, j/n, k/n)$ for $i, j, k \in \mathbb{N}$ and $i + j + k = n$ for some fixed n .



■ **Figure 4** The subtriangle $\Omega A_1 A_2$ is folded above t .

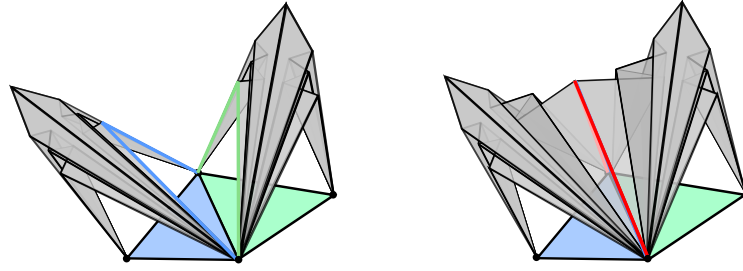
for $A_i A_j$ as in the lemma and so that the boundary edges $\Omega A_i, \Omega A_j$ are sent respectively to the segments $\omega' a_i$ and $\omega' a_j$. To this end, we first fold $\Omega A_1 A_2$ along its altitude from Ω and place the resulting two-winged shape above t so that the side $A_1 A_2$ is folded onto the broken line $a_1 m_{12} a_2$. We next consider a plane Π_1 in the pencil generated by $a_1 a_2$ to reflect the part of the two-winged shape lying to the right of that plane. See Figure 5. Another plane Π_2 in



■ **Figure 5** a, the reflection plane Π_1 . b, after reflection in Π_1 , and the plane Π_2 . c, reflection in Π_2 . d, after an even number of reflections the point Ω is sent to ω' .

the same pencil is then chosen to reflect part of the already reflected part. Choosing Π_1 and Π_2 appropriately, it is not hard to see that after an even number of such reflections the point Ω in $\Omega A_1 A_2$ will be sent to ω' . We finally apply the same construction to the two other subtriangles $\Omega A_2 A_3$ and $\Omega A_3 A_1$ and paste them to form a folding of T above t as desired.

► **Note 4.** This folding of T admits some flexibility. In particular, the boundary conditions can be modified so that each boundary wedge $a_i m_{ij} a_j$ is tilted around the axis $a_i a_j$. This allows to paste the constructions for two adjacent and non coplanar triangles; see Figure 6.



■ **Figure 6** Pasting two foldings of large triangles sharing an edge above smaller triangles that are non coplanar.

3.2 Embedding arbitrary polyhedral surfaces

Denote by $f : S \rightarrow \mathbb{E}^3$ the short C^2 map in Theorem 2. Let U be a union of small polygonal disks centered at each singular vertex of S . The strategy for the proof of Burago and Zalgaller is the following.

- (a) Compute an acute triangulation of $S \setminus U$, where each triangle is acute.
- (b) Compute an approximation f_1 of f that is almost conformal on $S \setminus U$ and short over S .
- (c) Refine the acute triangulation of $S \setminus U$ uniformly to obtain an acute triangulation \mathcal{T} with small triangles. The meaning of *small* depends on the geometric properties of f_1 and on the flexibility in Note 4.
- (d) Replace f_1 by its PL approximation F mapping linearly each triangle $T = A_1A_2A_3$ of \mathcal{T} to the triangle $F(T) := f_1(A_1)f_1(A_2)f_1(A_3)$ in \mathbb{E}^3 .
- (e) Apply the construction in Section 3.1 to every pair $(T, F(T))$, using the tilted version in Note 4 in order to paste the constructions of adjacent triangles.
- (f) Fill the gaps corresponding to U with specific constructions to deal with singularities as described in [3].

We refer to the full version on ArXiv and to the original paper [3] for more details.

4 Embedding flat tori

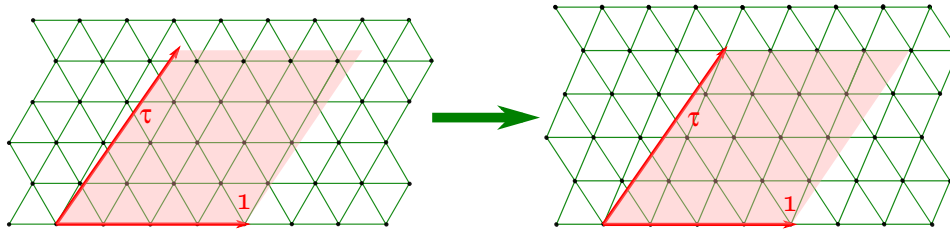
Step (b) in the proof of Burago and Zalgaller is highly non constructive, and to our knowledge no explicit PL isometric embedding of a closed surface according to their method was known up to date. It appears that the steps of their construction can be greatly simplified in the case of flat tori. Thanks to these simplifications we were able to visualize PL isometric embeddings of various flat tori in \mathbb{E}^3 .

We first observe that there is no need for Step (f) since a flat torus has no singular vertex: the angles at the four corners of its defining parallelogram add up to 2π , showing that the only vertex after the side gluing is non singular. In particular, one should set $U = \emptyset$ in all the steps.

4.1 Acute triangulation of flat tori

Itoha and Yuan [4] have shown that every flat torus can be triangulated into at most 16 acute triangles. However, since we need a fine triangulation as in Step (c) with a good control on the acuteness, we use the following triangulation, which is conceptually simpler. Let τ be the modulus of the flat torus $\mathbb{T}_\tau := \mathbb{E}^2 / (\mathbb{Z}\tau + \mathbb{Z}e_1)$ (we abusively identify the plane with the complex numbers). We consider the equilateral triangular lattice generated by $e^{i\pi/3}/n$ and $1/n$ for some positive integer n . This lattice comes with a regular triangulation \mathcal{T}_e by equilateral triangles. Let $p_{a,b} = ae^{i\pi/3}/n + b/n$, with $a, b \in \mathbb{Z}$, be a point in this lattice that is closest to τ . In particular, $|\tau - p_{a,b}| \leq (n\sqrt{3})^{-1}$. We deform \mathcal{T}_e by a linear transformation

ℓ defined by $1 \mapsto 1$ and $p_{a,b} \mapsto \tau$. By the previous inequality and for n large enough, ℓ is close to the identity. The triangles in $\ell(\mathcal{T}_e)$ are thus close to equilateral. Now, the lattice $\mathbb{Z}\tau + \mathbb{Z}e_1$ leaves $\ell(\mathcal{T}_e)$ invariant, so that $\ell(\mathcal{T}_e)/(\mathbb{Z}\tau + \mathbb{Z}e_1)$ is a well defined triangulation of \mathbb{T}_τ by almost equilateral triangles. See Figure 7.



■ **Figure 7** The equilateral triangular lattice (here with $n = 4$) is deformed to fit the lattice of \mathbb{T}_τ .

4.2 Conformal embedding of flat tori

Theorem 2 requires an initial short C^2 embedding, further approximated in Step (b) by an almost conformal map. In the case of flat tori we can directly provide a short conformal embedding. We rely on the Hopf tori developed by Pinkall [7]. These are based on the Hopf fibration

$$p : \mathbb{S}^3 \rightarrow \mathbb{S}^2, (x, y, z, t) \mapsto (2xz + 2yt, 2xt - 2yz, x^2 + y^2 - z^2 - t^2),$$

a standard projection of the 3-sphere \mathbb{S}^3 onto the 2-sphere \mathbb{S}^2 whose fibers (the sets $p^{-1}(s)$ for $s \in \mathbb{S}^2$) are circles. Pinkall proves that if γ is a simple closed curve on \mathbb{S}^2 , then $p^{-1}(\gamma)$ is a flat torus isometric to \mathbb{T}_τ with $\tau = (A + iL)/(4\pi)$, where L is the length of γ and A is the oriented area delimited by γ on \mathbb{S}^2 , choosing the side of γ so that $A \in [-2\pi, 2\pi)$. Since this torus lies in $\mathbb{S}^3 \subset \mathbb{E}^4$, it remains to apply a stereographic projection, say from the South pole $(0, 0, 0, -1)$, assuming it does not lie on the torus, to obtain a conformal embedding of \mathbb{T}_τ in \mathbb{E}^3 . In coordinates: $(x, y, z, t) \mapsto (x, y, z)/(t + 1)$.

Banchoff [2] revisited Pinkall’s approach to give explicit parametrizations of the Hopf-Pinkall tori. On \mathbb{S}^2 , Banchoff considers a curve of the form $\gamma_\tau(\theta) = (\sin \phi(\theta)e^{i\theta}, \cos \phi(\theta))$ given in spherical coordinates, where the polar angle $0 < \phi < \pi$ is a smooth function of the azimuthal angle $0 \leq \theta \leq 2\pi$. He next defines $L(\theta) = \int_0^\theta |\gamma'_\tau(t)| dt$ to be the length of the curve portion $\gamma_\tau([0, \theta])$ and $A(\theta) = \int_0^\theta (1 - \cos \phi(t)) dt$ the area on \mathbb{S}^2 swept by the arc of meridian linking the North Pole to the point on γ_τ up to θ . The conformal embedding $f_\tau : \mathbb{T}_\tau \rightarrow \mathbb{E}^3$ is then given by $f_\tau = f \circ g^{-1}$ with

$$f : (\mathbb{R}/2\pi\mathbb{Z})^2 \rightarrow \mathbb{E}^3, (\theta, \psi) \mapsto \left(\sin \frac{\phi(\theta)}{2} e^{i(\theta+\psi)}, \cos \psi \cos \frac{\phi(\theta)}{2}, \sin \psi \cos \frac{\phi(\theta)}{2} \right), \text{ and}$$

$$g : (\mathbb{R}/2\pi\mathbb{Z})^2 \rightarrow \mathbb{T}_{-1/\tau} \sim \mathbb{T}_\tau, (\theta, \psi) \mapsto \left(\frac{L(\theta)}{2}, \frac{A(\theta)}{2} + \psi \right).$$

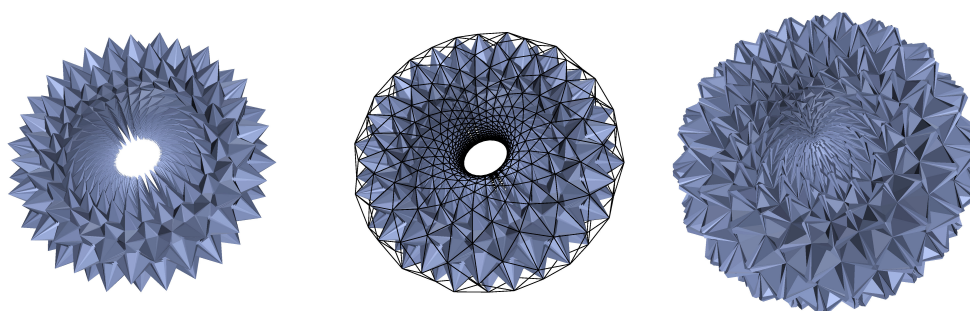
We have chosen ϕ of the form $\phi(\theta) = a + b \sin(n\theta)$ for $a < b, 0 \leq b < \pi - a$ and $n \in \mathbb{N}$. In order to represent the modulus $\tau = \tau_1 + i\tau_i$, the parameters a, b, n should satisfy $A(2\pi) = 4\pi\tau_1$ and $L(2\pi) = 4\pi\tau_i$, or equivalently:

$$J_0(b) \cos(a) = 1 - 2\tau_1 \quad \text{and} \quad \int_0^{2\pi} \sqrt{n^2 b^2 \cos^2(nt) + \sin^2(a + b \sin(nt))} dt = 4\pi\tau_i,$$

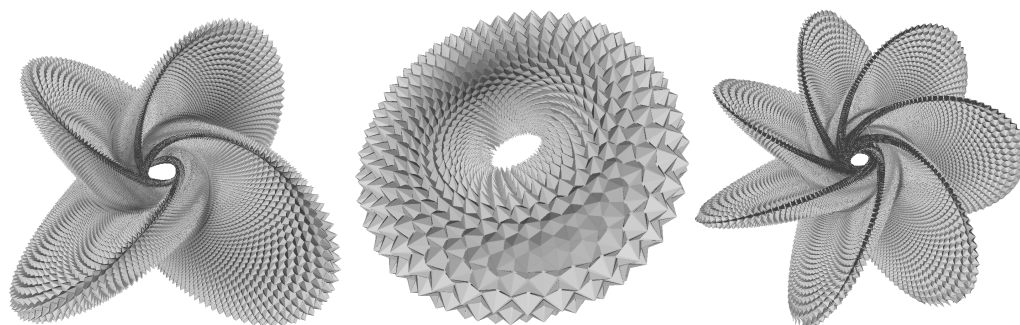
where $J_0(b) = \frac{1}{\pi} \int_0^\pi \cos(b \sin t) dt$ denotes the 0-th Bessel function of the first kind. The condition on the total area implies $0 \leq \tau_1 \leq 1$. Nevertheless, it is still possible to obtain a conformal embedding in the case of $\tau_1 < 0$ by first reflecting the torus along one of its boundary edge and applying a reflexion of the image torus in \mathbb{E}^3 . We can thus cover the whole moduli space.

4.3 The final construction

We now have all the pieces to produce PL isometric embedding of flat tori. Given a modulus τ , we first compute a quasi-equilateral triangulation of \mathbb{T}_τ as in Section 4.1. We then compute a PL approximation F_τ of the conformal map f_τ defined in Section 4.2 and finally apply the construction in Section 3.1 to every pair of triangles $(T, F_\tau(T))$. Figures 8 and 9 show some results.



■ **Figure 8** Left, PL isometric embedding of the square flat torus with 170,040 triangles. Middle, the mesh with black edges shows the PL approximation of the initial almost conformal embedding. Each of its triangles is replaced with a construction (in blue) as in Section 3.1 oriented toward the interior of the initial embedding. Right, The construction is oriented towards the outside, giving another isometric immersion of the square torus. (This last model has self-intersections. A finer triangulation should be used to avoid them.)



■ **Figure 9** isometric immersion of \mathbb{T}_τ with, from left to right, $\tau = e^{i\pi/3}, (1+i)/2, (1+3i)/2$. The left immersion is a hexagonal torus. While the subdivisions of the left and right tori already contain more than 7 millions triangles, they present self-intersections. A finer triangulation should be used to get an embedding.

5 Universal triangulation

The construction of Burago and Zalgaller gives rise to triangulations with a huge number of triangles, moreover distinct for every flat torus. In order to get a unique abstract triangulation that admits linear embeddings in \mathbb{E}^3 isometric to *any* flat torus, we resort to a second construction by Zalgaller [10] and to very recent work by Tsuboi [9] and Arnoux et al. [1] for embedding flat tori.

5.1 Embedding long tori

Any flat torus can be obtained by identifying abstractly the top and bottom boundaries of a right circular cylinder. We obtain non-rectangular tori by shifting circularly the top boundary before identification. We can moreover cover all the torus moduli by varying the ratio between the height of the cylinder and the length of its boundaries. A torus is said **long** when this ratio is large. In [10], Zalgaller proposes an origami style folding of long flat tori, much simpler than the general construction of [3]. Here, we quantify how long should be a torus to allow for the Zalgaller folding, and we show that the long tori admit a universal triangulation.

► **Proposition 5.** *There exists an abstract triangulation with 270 triangles, which admits linear embeddings isometric to every torus of modulus $\tau_1 + i\tau_2$ with $\tau_2 \geq 33$.*

The proof reduces to a careful analysis of the construction of Zalgaller. Instead of a circular cylinder, Zalgaller starts with a polyhedral cylinder in \mathbb{E}^3 , namely a prism with equilateral triangular basis, that he bends at several places to make the boundaries coincide, allowing their geometric identification. A twist is also applied before the bending so as to simulate a circular shift of the top boundary. In general, except for a twist of $2k\pi/3$, one boundary will be rotated with respect to the other after the twisting and bending, preventing their identification. Zalgaller then introduces a third modification that he calls a **gasket** in order to rotate a cross section of the prism without rotating the “material” of the prism. Intuitively, one should imagine a sleeve made of some non-elastic fabric, closed by two rigid triangles at the extremities. The right prism results from pulling tight on the triangles. Now, the effect of a gasket is to rotate one triangle around the axis of the prism, allowing the fabric to *slide* along the edges of this triangle.

How to bend a triangular prism

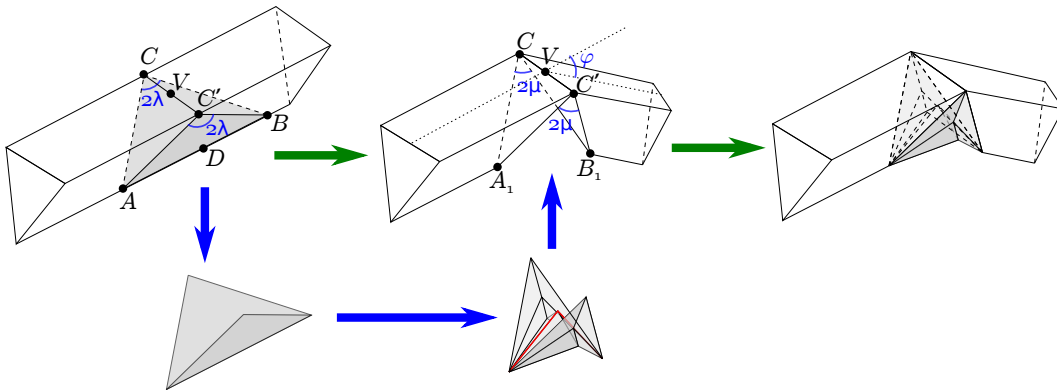
Consider a right prism \mathcal{P} with equilateral triangular basis and an orthogonal cross section $CC'D$. A **bending at an angle φ with cutting angle λ** along the **rib** CC' is obtained by (refer to Figure 10)

- (a) cutting two isosceles triangles ACB and $AC'B$ out of \mathcal{P} , where A, B lie on the generatrix of the prism through D , and the angle at C (and C') is 2λ ,
- (b) bending the cut prism at angle $0 < \varphi < \pi$,
- (c) folding ACB and $AC'B$ appropriately to fit them back on the bended prism.

Let A_1, B_1 be the respective positions of points A, B after bending and let $\angle A_1CB_1 = 2\mu$. In order for the construction not to overlap, one should have $\mu > 0$, hence λ should satisfy $\lambda_0(\varphi) < \lambda < \frac{\pi}{2}$ where $\lambda_0(\varphi)$ is the angle for which, after bending, the triangles A_1CC' and B_1CC' coincide. Looking at the right angled triangles ADC and ADV , one easily computes¹

$$\lambda_0(\varphi) = \arctan\left(\frac{\sqrt{3}}{2} \tan \frac{\varphi}{2}\right). \quad (1)$$

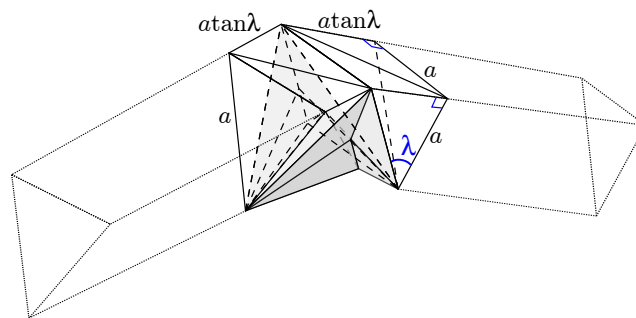
¹ This expression is simpler than the formula given in [10].



■ **Figure 10** Bending of a prism.

► **Lemma 6.** For every $\varphi \in (0, \pi)$ and for every $\lambda \in (\lambda_0(\varphi), \pi/2)$, there is an embedded bending of \mathcal{P} at angle φ with cutting angle λ introducing 12 triangles.

See the full version for a proof. For further reference, we call a **bend** a bent prism cut by orthogonal cross sections at the extremity of the above construction as on Figure 11.



■ **Figure 11** A bend is isometric to a right prism of length $2a \tan \lambda$.

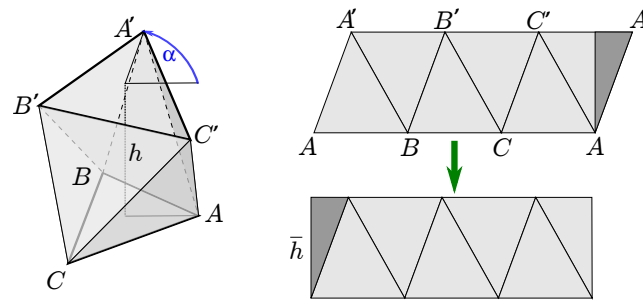
After triangulating the two top quadrilaterals, a bend is made of 20 triangles including the 12 triangles as in Lemma 6.

Rotating a cross section with a gasket

The ribs of the prism \mathcal{P} may have only three possible directions. This prevents to bend \mathcal{P} in an arbitrary direction. To circumvent this rigidity, Zalgaller introduces a simple construction that he calls a gasket. Consider an equilateral triangle ABC in the horizontal plane and a vertical translate $A'B'C'$ by height h . Rotate $A'B'C'$ by an angle α about the central vertical axis. The **gasket with turn α and height h** is the polyhedral cylinder formed by the six congruent triangles ABA' , $A'BB'$, $B'BC'$, $B'CC'$, $C'CA'$, $AA'C'$. See Figure 12. This gasket is embedded for every $\alpha \in (-\pi/3, \pi)$, independently of $h > 0$.

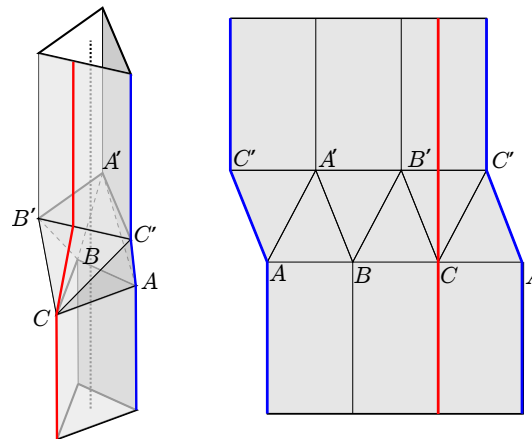
► **Lemma 7.** For every $\alpha \in (-\pi/3, \pi)$, the gasket with turn α and height h is isometric to a right prism of length \bar{h} with

$$\bar{h}^2 = h^2 + \frac{2}{27}(\sin^2 \frac{\alpha}{2} + \sin^2(\frac{\pi}{3} - \frac{\alpha}{2})) - \frac{4}{81}(\sin^2 \frac{\alpha}{2} - \sin^2(\frac{\pi}{3} - \frac{\alpha}{2}))^2 - \frac{1}{36} < h^2 + \frac{1}{9}. \quad (2)$$



■ **Figure 12** Left, a gasket with turn α and height h . Right, the gasket is unfolded in the plane. Cutting and pasting a small triangular piece shows that the gasket has the geometry of a right prism.

By pasting two prisms at the boundaries of a gasket, we obtain a polyhedral cylinder with triangular boundaries, where the two boundaries are turned at the angle α with respect to each other; see Figure 13.



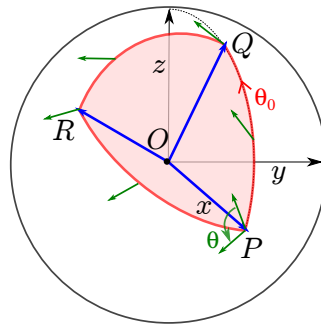
■ **Figure 13** Joining a gasket with two prisms to rotate their ribs. Right, unfolding of the construction showing the line of cut (in blue) and a generatrix (in red) of the polyhedral cylinder.

► **Note 8.** The top and bottom prisms in Figure 13 have the same central axis. This allows to rotate the rib of a prism at an angle $\alpha \in (\pi/3, \pi)$ before applying a bending.

► **Note 9.** By joining k gaskets in a row, we can rotate the rib of a prism at an angle $\alpha \in (-k\pi/3, k\pi)$.

Twisting a prism

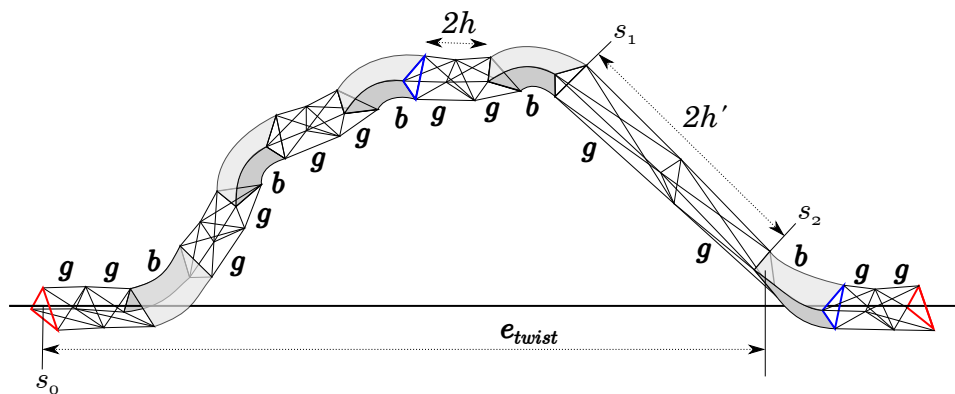
Replacing a portion of a prism by a gasket with turn α allows to turn one boundary, say the top one, of the prism with respect to the other one but does not *twist* the geometry: the top endpoint of a geodesic line perpendicular to the bottom boundary (a generatrix) will glide along the top boundary as we augment α . In order to twist the prism so that the top endpoint of this geodesic line indeed turns with the boundary, Zalgaller introduces yet another construction that he calls a **helical twist**. This construction takes advantage of the holonomy of parallel transport on the sphere: consider a unit sphere of center O with a spherical triangle PQR (see Figure 14). If one parallel transports an object from P to P



■ **Figure 14** The green tangent vector is transported along the spherical triangle PQR . The angle θ is equal to the area of PQR , while the angle θ_0 is given by L'Huillier's formula.

following the sides of the triangle PQR , then the object is rotated by a certain angle around the axis OP which is equal to the signed area of the spherical triangle PQR . In order to twist a prism with axis directed by \vec{OP} by an angle θ we may thus bend the prism successively in the directions \vec{OQ} , \vec{OR} and \vec{OP} again. Each bending at angle φ indeed corresponds to a transport along a spherical geodesic of length φ . Each portion of prism between two bends should include two gaskets to orient its rib properly. Indeed, by Note 9, two gaskets allow to turn by an angle in $(-2\pi/3, 2\pi)$, which covers all the possible orientations.

A **helical twist of angle θ** consists of a sequence of gaskets and bends according to the pattern $(g^2b)^5g^2 = (g^2b)^3(g^2b)^2g^2$, where b, g stand respectively for bends and gaskets. The prefix $(g^2b)^3$ in the pattern is used to simulate the parallel transport as described above, assuming that the central axis of the initial cross section is already aligned with \vec{OP} . The next factor $(g^2b)^2$ allows to return on the central axis of the initial cross section. Since \vec{OP} is aligned with this central axis, the changes of direction due to the factor $(g^2b)^2$ happen in the same plane. The resulting holonomy is thus trivial. Finally, the last two gaskets allows to turn the cross section by any angle in $(-2\pi/3, 2\pi]$; see Figure 15.



■ **Figure 15** The cross section (in blue) after the last bending of a helical twist is rotated by an angle θ about the central axis with respect to the initial cross section (in red). The last two gaskets allow to turn the last cross section (in red) to be a translate of the first one.

In practice, to construct a helical twist of angle $\theta \in (-\pi, \pi]$, we choose an equilateral triangle PQR on the unit sphere, with area θ . Moreover, we fix $P = (1, 0, 0)$, and we take Q in the plane Oxz with positive z coordinate. Then, R is the unique point making PQR equilateral and counterclockwise. Denote by θ_0 the angle between the vectors \vec{OP} and

\overrightarrow{OQ} . By L'Huilier's formula, θ_0 satisfies the equation $4 \arctan \left(\sqrt{\tan(\frac{3}{4}\theta_0) \tan^3(\frac{\theta_0}{4})} \right) = \theta$. Traveling along PQR in trigonometric direction induces a positive rotation angle, while traveling clockwise induces a negative rotation angle. For $|\theta| \leq \pi$, L'Huilier's formula implies $\theta_0 < 1.92$. From (1), we deduce that the corresponding cutting angle satisfies $\lambda < \lambda_0 := 0.89$. Denote by s_0 the initial cross section of the helical twist, by s_1 the cross section at the end of the fourth bend, and by s_2 the initial cross section of the last bend. Refer to Figure 15.

► **Lemma 10.** *Given any twist angle $\theta \in (-\pi, \pi]$ and any $h > 0$, we can construct a helical twist of angle θ so that all its bends have cutting angle λ_0 , and all its gaskets have height h , except the two gaskets between sections s_1 and s_2 , which have height h' imposed by our construction. This helical twist is isometric to a right prism with length*

$$\ell_{twist} = 10a \tan \lambda_0 + 10\bar{h} + 2\bar{h}'$$

and the horizontal distance between the boundaries of the helical twist is bounded by

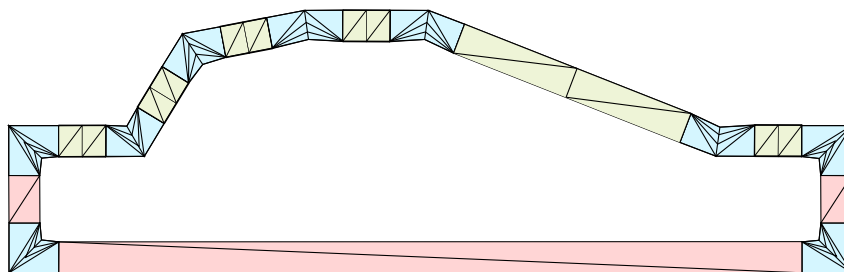
$$d_{twist} = 18(a \tan \lambda_0 + h).$$

Here, \bar{h} and \bar{h}' are given by Equation (2). The height h' is moreover bounded by $2\sqrt{10}(2h + 3a \tan \lambda_0)$.

See the full version for a proof.

Putting the pieces together

Consider a flat torus with modulus $\tau = \tau_1 + i\tau_i$. It can be obtained from a right circular cylinder of height τ_i and boundary length 1, identifying the boundaries after a circular shift at angle $2\pi\tau_1$. Zalgaller constructs his PL isometric embeddings of long tori, for which τ_i is large, as follows. He first replaces the circular cylinder by an isometric equilateral triangular prism that is bent 6 times at angle $\pi/3$ to form a hexagonal tube. If the torus is rectangular, that is if $\tau_1 = 0$, then the identification of the initial and final cross sections provides the desired embedding. Otherwise, he replaces one side of the hexagon by a helical twist of angle $2\pi\tau_1$ in order to glue the boundaries of the prism with the correct angular shift. We use a slightly different construction that allows us to get shorter tori. Starting from a helical twist of angle θ , we add 4 bends at angle $\pi/2$ and 3 portions of right prisms as illustrated on Figure 16 to form a closed torus. In order to avoid intersections between the horizontal prism and the horizontal gaskets of the helical twist we choose the two vertical prisms of



■ **Figure 16** Our construction decomposed into bends (in light blue), gaskets (in light green) and triangular prisms (in pink).

length $\frac{a}{3} > \frac{a}{2\sqrt{3}}$. We also choose the length of the horizontal prism to be equal to the total horizontal extent of the helical twist. We finally take the cutting angle of the 3 bends equals to $\lambda'_0 := \arctan(9/10) > \lambda_0(\pi/2)$. The resulting torus has length

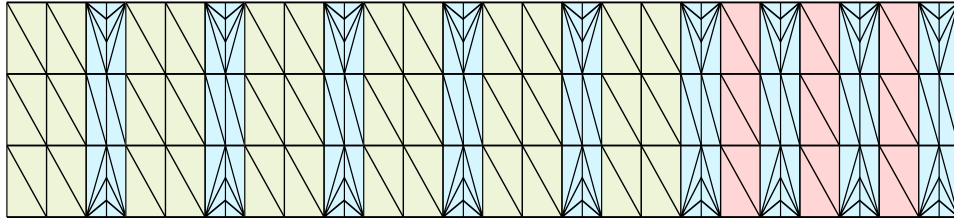
$$L < \ell_{\text{twist}} + 8a \tan \lambda'_0 + 2a/3 + d_{\text{twist}} = 28a \tan \lambda_0 + 8a \tan \lambda'_0 + 2a/3 + 18h + 10\bar{h} + 2\bar{h}',$$

where ℓ_{twist} and d_{twist} are given by Lemma 10. Using the bound for h' in Lemma 10 together with inequality (2), and the fact that $\tan \lambda_0 < 49/40$, and $\tan \lambda'_0 = 9/10$, we get

$$L < \frac{253}{18} + 18h + 10\sqrt{h^2 + \frac{1}{9}} + 2\sqrt{40(2h + \frac{49}{40})^2 + \frac{1}{9}}.$$

By taking $h = 0$ we thus obtain $L < \frac{253}{18} + \frac{10}{3} + 2\sqrt{\frac{49^2}{40} + \frac{1}{9}} < 33$. Note that any longer torus can be obtained by elongating the two vertical prisms. Hence, for h small enough, we can realize any flat torus of length at least 33. In practice, our implementation shows that the same construction allows to embed shorter tori. See Figure 19 in the full version.

We remark that a prism can be triangulated as a gasket with turn 0, the whole construction thus corresponds to the pattern $(g^2b)^5g^2(bg)^3b$ and is composed of $15 \times 6 + 9 \times 20 = 270$ triangles. This ends the proof of Proposition 5. Figure 17 shows the resulting unfolded triangulation after cutting through a cross section and a longitude.



■ Figure 17 A universal triangulation for long tori.

5.2 The flat tori of Tsuboi and Arnoux et al.

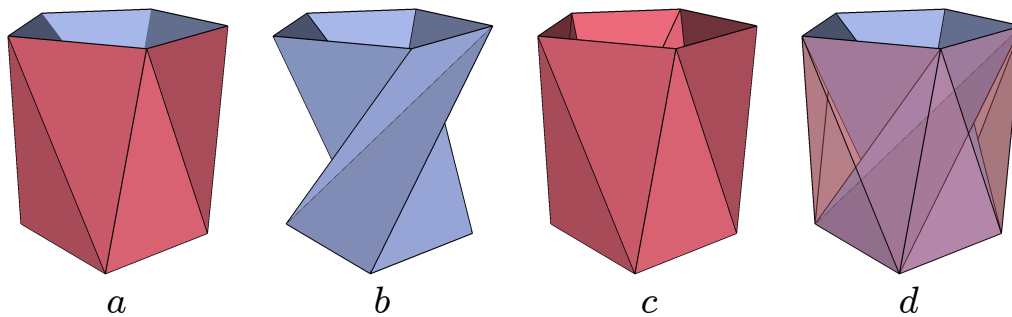
The previous construction provides a universal triangulation for long tori. Referring to Figure 1, this means that the part of the moduli space above the horizontal line $\tau_i = 33$ can be geometrically realized in \mathbb{E}^3 by this unique abstract triangulation. It thus remains to cover the compact subspace of *short tori* below this line. Denote this subspace by $\mathcal{M}_{\text{short}}$. Hence,

$$\mathcal{M}_{\text{short}} = \{\tau \in \mathbb{H}^2 \mid |\tau| \geq 1, |\tau_1| \leq 1/2, |\tau_i| \leq 33\}.$$

As already observed in Section 3, the construction of Burago and Zalgaller allows for some flexibility, implying that around every point in the moduli space there is a neighborhood that can be geometrically realized by the same abstract triangulation. By compactness we can cover $\mathcal{M}_{\text{short}}$ with a finite number of such neighborhoods. We could thus overlay all the corresponding triangulations with the universal triangulation for long tori to obtain a universal triangulation for all tori. This already provides a proof of the existence of such a triangulation. However, estimating the size of the neighborhoods seems impractical and the approach would lead to a gigantic triangulation. Surprisingly, it was only very recently that Tsuboi [9] and Arnoux et al. [1] independently (re)discovered extremely simple geometric

realizations of flat tori. Arnoux et al. are able to prove that their construction, that they call *diplotorus*, allows to realize all tori in the moduli space. For completeness we briefly recall this construction.

The diplotorus $\mathcal{D}_{n,d}^{a,h}$ with parameters n, d, a, h is defined as follows. Let $A_k = (e^{i\frac{2\pi k}{n}}, 0)$ be the vertices of the regular n -gon in the horizontal coordinate plane. Let $B_k = (e^{i\frac{\pi}{n}(a+1+2k)}, h)$ be the vertices of the vertical translate by h of this n -gon, turned by an angle $(a + 1)\frac{\pi}{n}$. Then $\mathcal{D}_{n,d}^{a,h} = \mathcal{P}_{\text{int}} \cup \mathcal{P}_{\text{ext}}$ is the union of two twisted prisms, called *ploids*, where \mathcal{P}_{int} is the union of triangles $\{A_k A_{k+1} B_k\}_{0 \leq k < n}$ and $\{B_k A_{k+1} B_{k+1}\}_{0 \leq k < n}$, and \mathcal{P}_{ext} is the union of triangles $\{A_k A_{k+1} B_{k-d}\}_{0 \leq k < n}$, $\{B_{k-d} A_{k+1} B_{k+1-d}\}_{0 \leq k < n}$. Of course, all the indices should be considered modulo n . Figure 18 shows the diplotorus $\mathcal{D}_{5,2}^{3.5,2}$.



■ **Figure 18** View of the diplotorus $\mathcal{D}_{5,2}^{3.5,2}$ (a) with its internal (b) and external (c) ploids. (d), another view of $\mathcal{D}_{5,2}^{3.5,2}$ with a transparent external ploid.

► **Lemma 11** (Arnoux et al., 2021). *For $h, a \in \mathbb{R}$ and $n, d \in \mathbb{Z}$, $\mathcal{D}_{n,d}^{a,h}$ is an embedded flat torus if and only if*

$$h > 0, n > 4, 2 \leq |d| < n - 2, d + 1 < a < n - 1 \text{ if } d > 0, \quad \text{and} \quad 1 - n < a < d - 1 \text{ if } d < 0$$

Moreover, the modulus of $\mathcal{D}_{n,d}^{a,h}$ is $\tau(n, d, a, h) = \tau_1(n, d, a) + i\tau_i(n, d, a, h)$ with

$$\tau_1(n, d, a) = d/n - \frac{\cos((a - d)\frac{\pi}{n}) \sin(d\frac{\pi}{n})}{n \sin \frac{\pi}{n}} \quad \text{and}$$

$$\tau_i(n, d, a, h) = \left(\sqrt{h^2 + 4 \sin^2\left(\frac{a+1}{2} \cdot \frac{\pi}{n}\right) \sin^2\left(\frac{a-1}{2} \cdot \frac{\pi}{n}\right)} + \sqrt{h^2 + 4 \sin^2\left(\frac{a-2d+1}{2} \cdot \frac{\pi}{n}\right) \sin^2\left(\frac{a-2d-1}{2} \cdot \frac{\pi}{n}\right)} \right) / (2n \sin(\pi/n))$$

For n, d fixed, we denote by $\mathcal{M}_{n,d}$ the moduli space of the tori $\mathcal{D}_{n,d}^{a,h}$. It lies above the graph of the parametrized curve $a \mapsto (\tau_1(n, d, a), \tau_i(n, d, a, 0))$, where a varies as in Lemma 11.

5.3 Realizing the short tori with three diplotori

The fundamental domain in Figure 1 is symmetric with respect to the imaginary axis. Two symmetric points τ and $-\bar{\tau}$ actually represent isometric tori, but the isometry should reverse the orientation. Hence, if \mathbb{T}_τ has a PL isometric embedding in \mathbb{E}^3 so does $\mathbb{T}_{-\bar{\tau}}$: just take a reflected image of the embedding of \mathbb{T}_τ . It is thus enough to realize the positive part $\mathcal{M}_{\text{short}}^+ := \{\tau \in \mathcal{M}_{\text{short}} \mid \tau_1 \geq 0\}$ of the short tori to ensure that we can realize all of them.

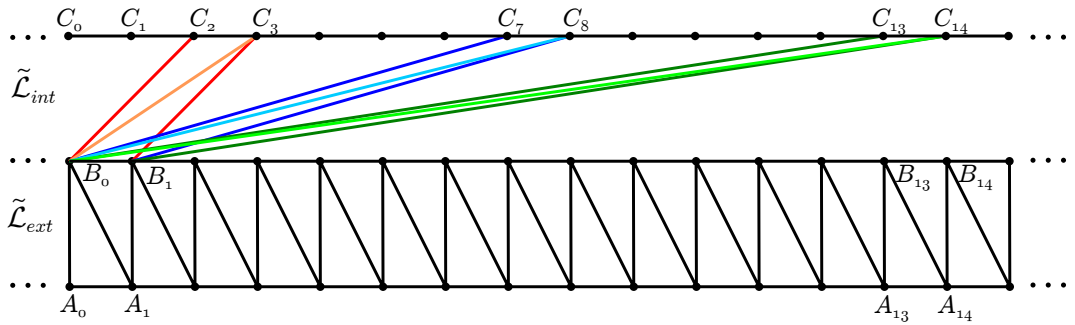
► **Lemma 12.** *Any modulus in \mathcal{M}_{short}^+ can be geometrically realized by a diplotorus with parameters $n = 19$ and $d \in \{2, 7, 13\}$.*

The proof, deferred to the full version, amounts to show that $\mathcal{M}_{19,2} \cup \mathcal{M}_{19,7} \cup \mathcal{M}_{19,13}$ indeed covers all the short tori.

From Lemma 12 we can construct a universal triangulation for short tori. Indeed, all the diplotori with fixed parameters n, d have the same abstract triangulation, that we denote by $\mathcal{T}_{n,d}$. Hence, we just need a common subdivision of $\mathcal{T}_{19,2}$, $\mathcal{T}_{19,7}$ and $\mathcal{T}_{19,13}$ to obtain such a universal triangulation. These triangulations are obtained by identifying the boundaries of a same triangulated cylinder. However, they are not isomorphic, as one needs to apply distinct circular shifts before identification. We can nonetheless send them in a *same* torus as follows. For $k \in \mathbb{Z}$, consider the points

$$A_k = (k, -1), \quad B_k = (k, 0), \quad C_k = (k, 1)$$

in the infinite plane strip $\mathcal{B} := \mathbb{R} \times [-1, 1]$. Then, $\mathcal{T}_{19,d}$ is isomorphic to the triangulation of \mathcal{B} by the triangles $\{A_k A_{k+1} B_k, B_k A_{k+1} B_{k+1}, C_k C_{k+1} B_{k-d}, B_{k-d} C_{k+1} B_{k+1-d}\}_{k \in \mathbb{Z}}$ quotiented by the horizontal translations generated by the vector $(n, 0)$, further identifying the two boundaries according to the vertical translation $(0, 2)$. This quotient and identification being independent of d , the three triangulations for $d = 2, 7, 13$ are indeed embedded in a same torus; see Figure 19.



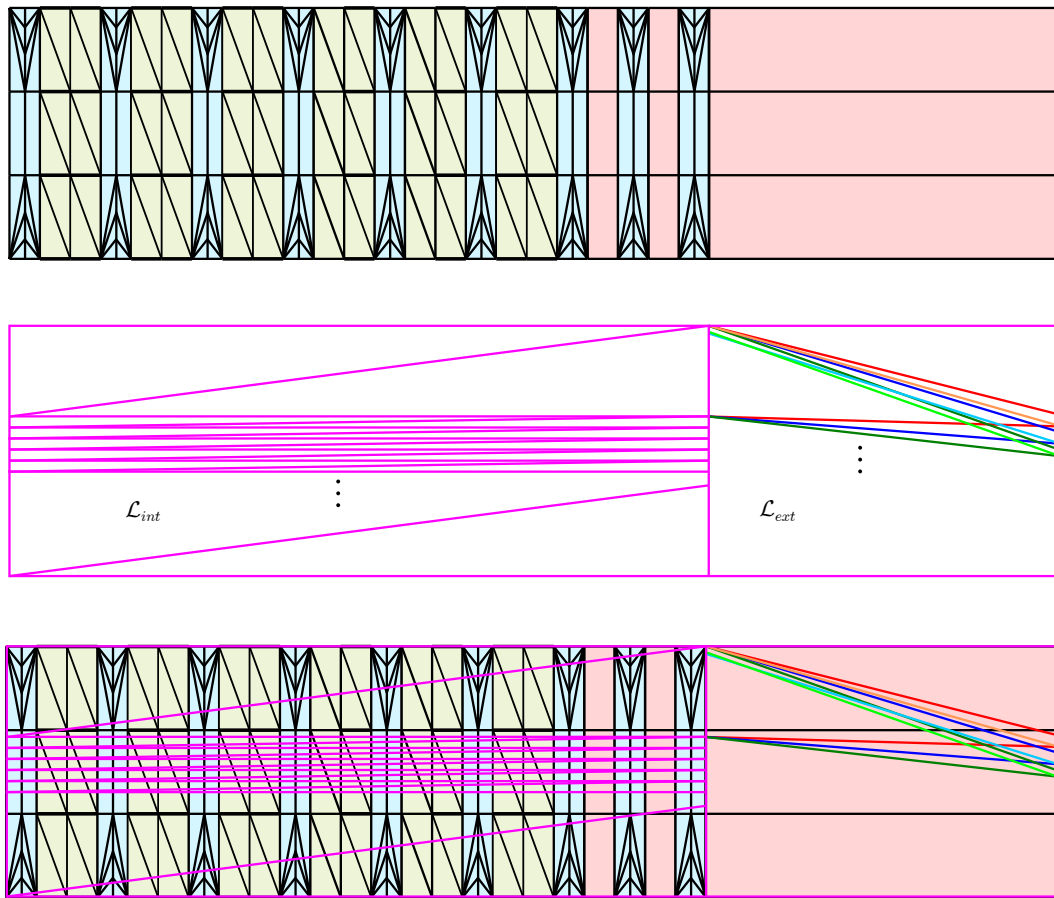
■ **Figure 19** Layout of the triangulations $\mathcal{T}_{19,2}$, $\mathcal{T}_{19,7}$ and $\mathcal{T}_{19,13}$. The two sub-strips $\tilde{\mathcal{L}}_{int}$ and $\tilde{\mathcal{L}}_{ext}$ correspond to the (lift of) overlay of the internal and external ploids.

We overlay the three triangulated strips obtained for $d = 2, 7, 13$. We can count the number of vertices of the resulting subdivision. We only have to care about the edges $B_k C_L$, the other ones being common to the three triangulations. In the full version we show that these edges intersect in 1064 crossing points. Adding the remaining points A_k, B_k (C_k and A_k should be identified) we find a total of $1064 + 38 = 1102$ vertices. By Euler’s formula on the torus, we conclude that the triangulated overlay has 2204 triangles. We have proved

► **Proposition 13.** *There exists an abstract triangulation with 2204 triangles, which admits linear embeddings isometric to every short torus.*

6 Merging short and long tori

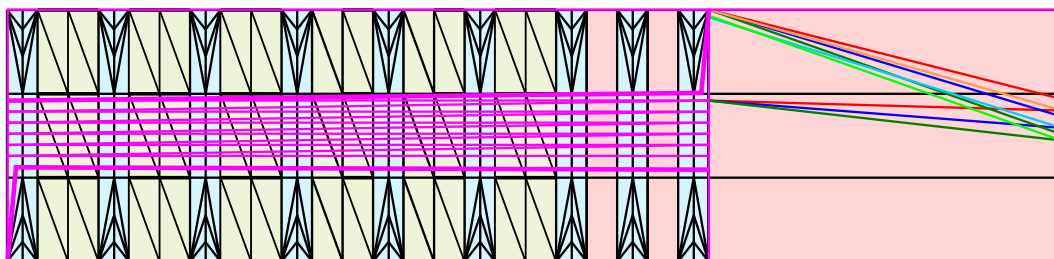
It remains to overlay our universal triangulations for long and short tori to obtain a universal triangulation for all tori. Before overlaying the layouts of Figures 17 and 19, we perform some modifications. We first remove the diagonals introduced to triangulate the rectangular



■ **Figure 20** Modified layout of the universal triangulations for long and short tori, and their overlay.

face of the bends as they are not necessary to define the isometric PL embeddings of long tori. For the same reason, we remove the diagonals used to triangulate the three portions of right prisms; See top Figure 20. Denote by $\mathcal{L}_{\text{long}}$ the resulting layout. We next apply a quarter turn to the layout for short tori, call it $\mathcal{L}_{\text{short}}$. It decomposes into two parts $\mathcal{L}_{\text{int}} \cup \mathcal{L}_{\text{ext}}$ corresponding to the internal and external ploids; See Figure 19. We apply some stretching and compression in order to align \mathcal{L}_{ext} with a portion of right prism in $\mathcal{L}_{\text{long}}$, and to concentrate all the vertices of $\mathcal{L}_{\text{short}}$, except the ones on the horizontal boundaries of the layout, in the central horizontal strip of $\mathcal{L}_{\text{long}}$. We can enumerate the vertices of the overlay as follows. It contains

- $V_{\cap} = 1064$ vertices from the intersecting edges in $\mathcal{L}_{\text{short}}$,
- $3V_{\text{ext}}$ vertices, where V_{ext} is the number of intersections in \mathcal{L}_{ext} of a horizontal edge of $\mathcal{L}_{\text{long}}$ with the edges of $\mathcal{L}_{\text{short}}$,
- $V_{\text{long}} = 270/2 = 135$ vertices from the triangulation of long tori,
- $(2n - 3)V_c = 35V_c$ vertices in the central horizontal strip, where V_c is the number of intersections of an edge of $\mathcal{L}_{\text{short}}$ in this strip with the edges of $\mathcal{L}_{\text{long}}$,
- V_d intersections of the two remaining diagonals of $\mathcal{L}_{\text{short}}$ with the edges of $\mathcal{L}_{\text{long}}$. Rather than considering these two diagonals as line segments, we subdivide each of them by adding a vertex close to their extremities, moving it to the boundary of the central strip; see Figure 21.



■ **Figure 21** The subdivision of the remaining two diagonals of $\mathcal{L}_{\text{long}}$ (thick purple lines).

In the full version of the paper we count $V_{\text{ext}} = 41$, $V_c = 45$, $V_d = 90$, leading to a total of 2987 vertices. By Euler's formula this corresponds, after adding diagonals to triangulate the overlay, to 5974 triangles. This ends the proof of Theorem 1.

Our construction is clearly not optimal. The size of our universal triangulation for long tori can probably be reduced by simplifying the helical twist. The overlay of the triangulation can also be optimized. A challenging question is to find the smallest number of triangles in a universal triangulation for flat tori.

References

- 1 Pierre Arnoux, Samuel Lelièvre, and Alba Málaga. Diplotori: a family of polyhedral flat tori. In preparation, 2021.
- 2 Thomas F. Banchoff. Geometry of the Hopf mapping and Pinkall's tori of given conformal type. In Martin C. Tangora, editor, *Computers in algebra*, volume 111 of *Lecture notes in pure and applied mathematics*, pages 57–62. M. Dekker, 1988.
- 3 Yuriy Dmitrievich Burago and Viktor Abramovich Zalgaller. Isometric piecewise-linear imbeddings of two-dimensional manifolds with a polyhedral metric into \mathbb{R}^3 . *Algebra i analiz*, 7(3):76–95, 1995. Transl. in *St Petersburg Math. J.* (7)3:369–385.
- 4 Jin ichi Itoha and Liping Yuan. Acute triangulations of flat tori. *European journal of combinatorics*, 30:1–4, 2009. doi:10.1016/j.ejc.2008.03.005.
- 5 Nicolaas Kuiper. On C^1 -isometric imbeddings. *Indagationes Mathematicae*, 17:545–555, 1955.
- 6 John F. Nash. C^1 -isometric imbeddings. *Annals of Mathematics*, 60(3):383–396, 1954. doi:10.2307/1969840.
- 7 Ulrich Pinkall. Hopf tori in S^3 . *Inventiones mathematicae*, 81(2):379–386, 1985. doi:10.1007/BF01389060.
- 8 Tanessi Quintanar. An explicit PL-embedding of the square flat torus into \mathbb{E}^3 . *Journal of Computational Geometry*, 11(1):615–628, 2020. doi:10.20382/jocg.v11i1a24.
- 9 Takashi Tsuboi. On origami embeddings of flat tori. *arXiv preprint*, 2020. arXiv:2007.03434.
- 10 V. A. Zalgaller. Some bendings of a long cylinder. *Journal of Mathematical Sciences*, 100(3):2228–2238, 2000. doi:10.1007/s10958-000-0007-3.